Carbon Capture Science & Technology 13 (2024) 100282

Contents lists available at ScienceDirect

Carbon Capture Science & Technology

journal homepage: www.elsevier.com/locate/ccst

Full Length Article

Boosting CO_2 selectivity by mono- and dicarboxylate-based ionic liquids impregnation into ZIF-8 for post-combustion separation

Tiago J. Ferreira[a], Thiago O. Carvalho[a], Joana Pais[a], Laura M. Esteves[a], Ludmila P.C. Silva[b], Patrícia M. Reis[a], José M.S.S. Esperança[a,*], Isabel A.A.C. Esteves[a,*]

[a] LAQV/REQUIMTE, Department of Chemistry, NOVA School of Science and Technology, FCT NOVA, 2829-516 Caparica, Portugal
[b] Departamento de Engenharia Química e de Petróleo, Universidade Federal Fluminense, Niterói, 24210-240, Brazil

ARTICLE INFO

Keywords:
Ionic Liquids (IL)
Metal-organic frameworks (MOF)
IL@MOF composites
CO_2/N_2 separation by selective sorption
CO_2 Post-combustion

ABSTRACT

Post-combustion carbon dioxide (CO_2) capture/separation is considered one of the main ways to minimize the impact of global warming caused by this greenhouse gas. This work used eight mono- and dicarboxylate-based ionic liquids (ILs) to impregnate metal-organic framework (MOF) ZIF-8. This anionic effect was studied for these mostly unreported IL@MOF composites to determine its impact on gas sorption and selectivity performance. Characterization results confirmed IL impregnation into the structure of ZIF-8, along with the conservation of microporosity and crystallinity in composites. Sorption-desorption equilibrium measurements were performed, and CO_2 and nitrogen (N_2) isotherms were obtained at 303 K for ZIF-8 and IL@ZIF-8 composites. At 0.15 bar, the dicarboxylate-based composite $[C_2MIM]_2[Glu]$@ZIF-8 showed the highest CO_2 gas sorption, showing 50 % more sorption capacity than the best monocarboxylate-base composites at this pressure. Dicarboxylate-based composites also showed remarkable N_2 sorption in the low-pressure range. The ideal CO_2/N_2 selectivity for a typical post-combustion composition was calculated, and a trend regarding the anionic carbon chain size was observed. The composite $[C_2MIM][Cap]$@ZIF-8 showed nearly five times more selectivity than the pristine ZIF-8 at 1 bar of total pressure. Dicarboxylate-based composites, given their low-pressure high N_2 sorption capacity, were not as selective as their respective monocarboxylate-based IL@ZIF-8 materials with the same carbon chain size.

1. Introduction

In the fight against global warming, there is an urgent need to peak carbon dioxide (CO_2) atmospheric emissions and achieve carbon neutrality to attain the Paris Agreement long-term temperature goals (Huang and Zhai, 2021). Different strategies can be considered to accomplish this, which include the use of renewable energies along with the more direct Carbon Capture and Storage (CCS) and Carbon Capture and Utilization (CCU) approaches. For the capture/separation stage of CCS/CCU, different technologies can be employed such as gas adsorption, gas absorption, membrane permeation, cryogenic distillation, and chemical looping, among others (Boot-Handford et al., 2014). In particular, gas adsorption is a low-energy demanding, environmentally friendly, and cost-effective technology when compared to more traditional processes like chemical amine scrubbing. The core of any adsorption process is the selection of the appropriate adsorbent which, for CCS purposes, should have high CO_2 adsorption capacity and/or be highly selective towards this gas.

With CO_2 capture/separation as the targeted application, the combination of metal-organic frameworks (MOFs) and ionic liquids (ILs) was proposed over a decade ago (Chen et al., 2011). These composite materials have been denominated IL@MOF or IL/MOF in the literature and can be considered as a type of supported ionic liquid phase (SILPs) materials.

MOFs are coordination networks made of metal cations or small metallic clusters and organic ligands that contain potential voids (Batten et al., 2013). They are considered an alternative to more traditional adsorbents, as generally they show very high specific surface area and total pore volume, chemical and structural tunability, thermal and chemical stabilities, and mild synthesis conditions, as well as high CO_2 adsorption (Baumann et al., 2019; Sumida et al., 2012). ILs are salts in the liquid state made of organic cations and organic/inorganic anions, with a melting point below 373 K. They have appealing physical and chemical properties such as negligible vapor pressure, nonflammability, and a high degree of tunability. These materials can show high CO_2 solubility, especially chemisorption ILs such as acetate-based ones (Carvalho et al., 2016).

* Corresponding authors.
E-mail addresses: jmesp@fct.unl.pt (J.M.S.S. Esperança), i.esteves@fct.unl.pt (I.A.A.C. Esteves).

https://doi.org/10.1016/j.ccst.2024.100282
Received 19 June 2024; Received in revised form 16 August 2024; Accepted 18 August 2024

Initial simulation studies indicated that the presence of confined ILs in MOFs would noticeably improve the selectivity towards CO_2, along with the sorption capacity of this gas between 0 and 1 bar (Chen et al., 2011; Vicent-Luna et al., 2013). Note that the term sorption is used herein to encompass both adsorption and absorption phenomena. As for the selectivity performance of these materials, composites turned out to be generally more selective than their pristine MOFs, and increasingly selective with higher IL loadings. It seemed that, irrespective of the chosen IL, both CO_2 sorption capacity and selectivity would improve for IL@MOF materials, between 0 and 1 bar.

However, unlike what was predicted by the simulation works, the increase in CO_2 sorption at this pressure has seldom been observed in experimental works. For example, our group picked ten different ILs with a reported affinity towards CO_2 and studied the influence of their cationic and anionic structures in the sorption capacity and selectivity performance of IL@MOF materials (Ferreira et al., 2019). The MOF used in this work was ZIF-8 and the same molar IL amount was impregnated so that direct comparisons between composites could be established. Considering the IL impregnation as a MOF "functionalization", it was observed that the sorption capacity and selectivity performance of the composites can be tuned according to the IL structure. Only one composite, impregnated with the acetate-based IL $[C_2MIM][Ac]$, was able to sorb more CO_2 than the pristine ZIF-8 between 0 and 1 bar, due to stronger solid-fluid interactions. The other composites were impregnated with physisorption ILs and sorbed less CO_2 than ZIF-8 in this pressure range. This trend has also been observed in other works that used physisorption ILs (da Silva et al., 2015; Zeeshan et al., 2018; Kavak et al., 2019; Mohamedali et al., 2019; Ferreira et al., 2020; Ferreira et al., 2022; Zeeshan et al., 2020).

A more recent simulation study (Xia et al., 2019), backed with experimental data, has revealed that models where the IL is randomly dispersed into the MOF structure are not suited to realistically describe the molecular structure of IL@MOF composites. These models were used in the initial simulation studies (Chen et al., 2011; Li et al., 2012). It was proposed the use of a blocked model where the IL gathers into specific sites of the MOF channels, hindering gas sorption. Simulated CO_2 isotherms of IL@MOF materials using the blocked model were closer to experimental results.

Gas sorption studies using IL@MOF materials have shown that these materials are promising for CO_2 post-combustion capture/separation. The gas is separated at ambient pressure from a flue gas mixture that mostly contains nitrogen (N_2), and where the CO_2 partial pressure is low (~0.15 bar) (Liang et al., 2017). That is because, while IL@MOF composites may sorb less CO_2 between 0 and 1 bar than their respective pristine MOF, the IL presence usually increases the selectivity performance of the material at this pressure range. At higher pressures, due to total pore volume loss, IL@MOF composites usually show less gas sorption capacity than their pristine MOF counterpart. Therefore, these materials are not so well-suited for high-pressure gas separations.

The primary effort of experimental gas sorption studies using IL@MOF has been to find out which IL should one impregnate to promote synergistic effects. A secondary studied aspect is how much these effects can be amplified by increasing the IL loading. Focusing on which ILs promote synergy for gas selectivity boosting, the literature indicates that $[NTf_2]^-$- [(Ban et al., 2015), $[PF_6]^-$- [(Kinik et al., 2016), $[N(CN)_2]^-$- (Zeeshan et al., 2018), amino acid- (Philip and Henni, 2022), bromide- (Pan et al., 2022), and carboxylate-based ILs (Ferreira et al., 2019; Mohamedali et al., 2019; Chen et al., 2018; Mohamedali et al., 2018; Mohamedali et al., 2019; Han et al., 2021) can be used to achieve this. Acetate-based ILs, namely $[C_2MIM][Ac]$ and $[C_4MIM][Ac]$, have been particularly studied in different MOFs, due to their strong anion-CO_2 interactions (chemisorption ILs) (Shi et al., 2014). However, this does not mean that acetate is the best anion to incorporate in an IL@MOF composite. Different carboxylate-based anions with longer chains, with additional functional groups or two carboxylic groups could just as well rival or even outperform the acetate anion.

In this work, eight monocarboxylate- and dicarboxylate-based ILs in total were impregnated through a direct contact method into MOF ZIF-8, considering a constant IL molar loading. ZIF-8 was chosen due to its properties, which include high specific surface area (~1800 m^2/g) and total pore volume (~0.65 cm^3/g), microporous nature (pore apertures of 3.4 Å and cavities of 11.6 Å), high thermal stability, and chemical stability in the presence of water (Venna and Carreon, 2010). Always using $[C_2MIM]^+$ as the cation, the anionic effect was studied to determine how the anion structure impacts sorbent properties like gas sorption capacity and selectivity performance of such composites. The influence of the anion chain size was considered, using short- (formate and acetate), medium-sized (valerate), and long-chained monocarboxylates (caprate). In addition, the presence of a ketone group in a medium-sized carboxylate (levulinate) was also studied, as high CO_2 sorption has been obtained with an IL containing this anion (Avila et al., 2021). Moreover, a fluorine-containing structural analogue of the acetate anion was also investigated (trifluoroacetate), to determine the impact of the fluorinated moiety. Finally, short (oxalate) and medium-sized dicarboxylates (glutarate) were tested to compare with their monocationic monocarboxylate analogues. To the best of the authors' knowledge, this is the first work where carboxylate-based dianionic ILs were considered to produce IL@MOF composites for gas sorption applications. Furthermore, apart from acetate-based composites, all the other IL@MOF materials produced herein have never been reported for gas sorption applications.

All IL@ZIF-8 materials were characterized with standard characterization techniques for powdered adsorbent materials. CO_2 and N_2 single-component sorption-desorption isotherms were obtained for pristine ZIF-8 and all composites to determine the gas sorption capacity of these materials. The measurements were performed at 303 K between 0 and 10 bar, using a highly accurate static gravimetric method already developed and detailed elsewhere (Ferreira et al., 2019; Esteves et al., 2008). With these data, ideal CO_2/N_2 selectivities were calculated through an accurate description of the sorption-desorption experimental data, using the Sips (Langmuir-Freundlich) and dual-site Sips isotherm models.

2. Materials and methods

2.1. Materials

MOF ZIF-8 was purchased from Sigma-Aldrich (commercial name Basolite® Z1200). The ILs $[C_2MIM]Br$ (1-ethyl-3-methylimidazolium bromide, 99 %), $[C_2MIM][Ac]$ (1-ethyl-3-methylimidazolium acetate, >98 %), $[C_2MIM][TfAc]$ (1-ethyl-3-methylimidazolium trifluoroacetate, >97 %) were acquired from IoLiTec GmbH. The other ILs were synthesized and purified in-house, namely $[C_2MIM][For]$ (1-ethyl-3-methylimidazolium formate, 99 %), $[C_2MIM][Val]$ (1-ethyl-3-methylimidazolium valerate, 99 %), $[C_2MIM][Lev]$ (1-ethyl-3-methylimidazolium levulinate, 99 %), $[C_2MIM][Cap]$ (1-ethyl-3-methylimidazolium caprate, 99 %), $[C_2MIM]_2[Oxa]$ (bis(1-ethyl-3-methylimidazolium) oxalate, 99 %) and $[C_2MIM]_2[Glu]$ (bis(1-ethyl-3-methylimidazolium) glutarate, 99 %). For their respective syntheses, formic acid (Honeywell, ≥98 %), valeric acid (Sigma-Aldrich, ≥99 %), levulinic acid (Sigma-Aldrich, 98 %), capric acid (Sigma-Aldrich, ≥98 %), oxalic acid (Sigma-Aldrich, 98 %) and glutaric acid (Sigma-Aldrich, 99 %) were purchased. Also, for ILs syntheses, acetone (Carlo Erba, 99.8 %), ultrapure water produced in-house with a WaterMax W1 equipment (Diwer Technologies), and diethyl ether (Honeywell, ≥99.8 %) were used. The ILs chemical structures are shown in Fig. 1, while their synthesis procedure can be found in the Supporting Information (SI), as well as their ^1H and ^{13}C NMR spectra (Figures S1-S12). To obtain the NMR spectra, deuterium oxide (D_2O, Eurisotop, 99.9 % D) was used as the assay solvent. Ethanol (99.9 %, Scharlau) was used to dissolve the ILs before their impregnation into the structure of ZIF-8. Potassium bromide (KBr, FT-IR grade, PanReac) was used to produce infrared solid sample-containing tablets to obtain infrared (FT-IR) spectra. For the sorption-desorption equilibria measurements, the gases

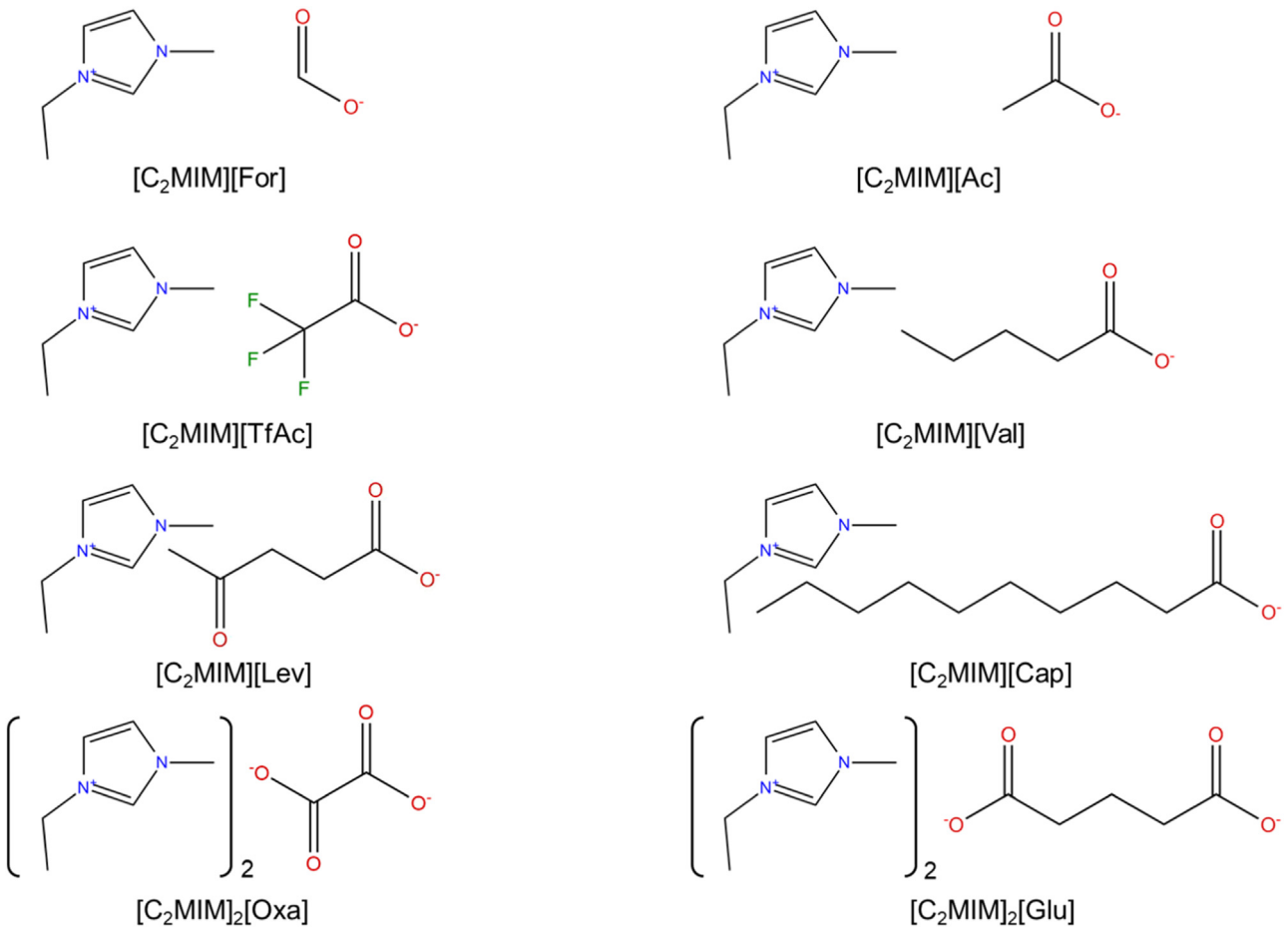

Fig. 1. Chemical structures of the ILs used in this work.

used in this work were CO_2 (99.998 %, Air Liquide), N_2 (>99.998 %, Praxair), and helium (He, ≥99.999 %, Air Liquide).

2.2. Composites preparation

[C_2MIM][Ac] was chosen as the work reference IL, and a 10 wt.% loading was defined. This weight loading corresponds to a molar loading (12.9 mol%) that was kept constant for all the produced IL@ZIF-8 composites. This allows direct and valid comparisons between the materials.

The production of the IL@ZIF-8 composites obeyed the experimental protocol previously reported by our group (Ferreira et al., 2019). All ILs were previously dried under vacuum for at least 48 h, at 0.1 Pa and 313 K. Generically, the IL was firstly weighed and later dissolved in ethanol at ambient temperature. This IL solution was stirred for 15 min. Afterward, 1 g of ZIF-8 (which was degassed for at least 4 h at 373 K to ensure the MOF is free from adsorbed impurities) was weighed in another vial. In the impregnation step, the IL solution was added to the MOF vial, capped, and stirred overnight at room temperature. The drying stage of this preparation included the uncapping of the vial, followed by slow solvent evaporation at 338 K. The final drying stage consisted in degassing the composite material at 373 K for 4 h to remove trace amounts of solvent.

2.3. Samples characterization

2.3.1. Fourier transform infrared (FT-IR) spectroscopy

A FT-IR Spectrometer Spectrum Two model (Perkin Elmer) was used to obtain the infrared spectra of pristine ZIF-8, neat ILs, and the produced composites. For the ILs, the Attenuated Total Reflectance (ATR) module was used. For the solid materials, a Transmittance module with KBr tablets containing an adequate amount of sample was used to obtain more defined assignments. The spectra were obtained under ambient-temperature conditions, between 4000 and 450 cm^{-1} (spectral resolution of 4 cm^{-1}).

2.3.2. Thermogravimetric analysis (TGA)

A thermogravimetric analyzer Labsys EVO (Setaram) was used to obtain the thermograms, of neat ILs, pristine ZIF-8, and IL@ZIF-8 composites. Each sample was held in an alumina sample pan and placed under a 50 mL/min flow of argon (Ar). It was initially heated until 373 K using a 10 K/min heating step, followed by an isothermal step at 373 K for 1 h. This ensured the removal of pre-adsorbed impurities and/or moisture, allowing the analyzed sample to be completely dry before the dynamic assay, which was performed up to 1273 K at a 10 K/min heating rate.

2.3.3. N_2 sorption-desorption equilibrium at 77K

A static volumetric apparatus ASAP 2020 (Micromeritics) was used to collect the N_2 sorption-desorption equilibrium isotherms at 77 K of ZIF-8 and IL@ZIF-8 composites. The sample degassing occurred under vacuum at 373 K for a minimum of 4 h, before the sorption-desorption measurement started. From the collected data, it was possible to determine the textural properties of these materials like total pore and micropore volumes, or BET/Langmuir specific surface areas. With the use of non-local density functional theory (NLDFT) calculations applied to the collected sorption-desorption data, it was possible to determine the pore size distribution (PSD) of the materials.

2.3.4. Powder X-ray diffraction (PXRD)

An X-ray diffractometer MiniFlex II (Rigaku) was used to obtain the powder X-ray diffractograms of pristine ZIF-8 and IL@ZIF-8 materials. The X-ray generator used a Cu radiation source with 30 kV voltage and 15 mA current. Assays were run between 2 ° and 50 °, step width of 0.02 ° and 0.5 °/min as the defined scanning speed.

2.4. Gas sorption-desorption equilibrium measurements

A standard gravimetric method was used to experimentally obtain the CO_2 and N_2 sorption-desorption equilibrium isotherms for pristine ZIF-8 and IL@ZIF-8 composites. Measurements were performed at 303 K, between 0 and 10 bar. The main feature of the gravimetric apparatus is a high-accuracy ISOSORP 2000 magnetic-suspension balance (Rubotherm GmbH). Before the measurements, samples were degassed for 4 h at 373 K, in situ and under vacuum. Details about the gravimetric apparatus and its schematic can be found elsewhere (Ferreira et al., 2019; Ferreira et al., 2020; Esteves et al., 2008).

Adsorbed gas amounts have been reported in the literature using net (q_{net}), excess (q_{exc}), or total adsorption (q_t) quantities. These quantities can still be applied for IL@ZIF-8 composites, where both gas adsorption and absorption will occur. In this work, the net quantity was considered. It is a recent concept that refers to the difference between the amount of sorbate found in a measurement cell with and without the presence of the sorbent (Gumma and Talu, 2010). The specific net amount sorbed (in mol gas/mass sorbent) is given as follows

$$q_{net}=\frac{m-m_s-m_h+V_h\rho_g}{m_s\ M_w}, \tag{1}$$

where m is the weighed mass that the balance registers, m_s is the degassed mass of sorbent inside the sample holder, and m_h and V_h are the mass and volume of the sample holder contributing to buoyancy effects, respectively. Also, ρ_g is the gas density at the measurement equilibrium pressure and temperature, assessed from NIST Chemistry WebBook, while M_w is the molecular weight of the sorbed gas. Net quantity removes the uncertainty that arises from the use of probe molecules (e.g., He, N_2) in the determination of the required reference state. Despite this, the mostly used in the literature is the total sorbed quantity (q_t). The three sorbed quantities (in mol gas/mass sorbent) are related as shown (Ferreira et al., 2019)

$$q_t=q_{exc}+V_p\rho_g=q_{net}+\left(V_p+V_s\right)\rho_g, \tag{2}$$

where $V_s = 1/\rho_s$ is the specific solid volume of the sorbent that is impenetrable to the sorbate, ρ_s is the skeletal density of the sorbent (its determination is made through He pycnometry), and V_p is the specific total pore volume of the sorbent material (determined from N_2 sorption-desorption at 77 K). In the case of composite materials, the above formula is valid if V_p and ρ_s account for the IL presence. The details of He pycnometry are disclosed elsewhere (Esteves et al., 2008).

The pure component sorption-desorption equilibrium data of pristine ZIF-8 were fitted using the Sips isotherm model, as it can be applied to microporous materials with homogeneous sorbent surfaces (Do, 1998)

$$q_t(P)=\frac{q_s(bP)^{1/n}}{1+(bP)^{1/n}}, \tag{3}$$

where P is the absolute pressure, q_s is the maximum sorbed amount, and b and n are affinity and heterogeneity parameters, respectively. For the IL@ZIF-8 composites, given the lack of classic Type I isotherms due to the impregnated ILs nature, the dual-site Sips isotherm model was used to fit the pure component sorption-desorption equilibrium data (Do, 1998)

$$q_t(P)=q_{s1}\frac{\left(b_1P\right)^{1/n_1}}{1+\left(b_1P\right)^{1/n_1}}+q_{s2}\frac{\left(b_2P\right)^{1/n_2}}{1+\left(b_2P\right)^{1/n_2}}, \tag{4}$$

where q_{s1} and q_{s2} are the maximum sorbed amount for the sorption sites 1 and 2, respectively, and b_1 and b_2 are the affinity constants of these sorption sites. This model assumes the material has sorption sites with different energies. The use of this model is appropriate for these IL@ZIF-8 composites, given the existence of both carboxylate IL and MOF sorption sites (Yang et al., 2021). The ideal selectivities of ZIF-8 and IL@ZIF-8 composites were calculated at 303 K for flue gas composition (assumed as 15 vol.% CO_2 and 85 vol.% N_2) following the equation (Do, 1998)

$$S_{\frac{CO_2}{N_2}}=\frac{q_{t\ CO_2}/q_{t\ N_2}}{p_{CO_2}/p_{N_2}}, \tag{5}$$

and taking into consideration the partial pressure, p_i, of each gas i.

3. Results and discussion

3.1. FT-IR spectroscopy

To confirm successful IL impregnation, FT-IR spectra of neat ILs and IL@ZIF-8 composites were compared. Figures S13-S20 (*See* SI) showed that the ZIF-8 FT-IR data are in agreement with that reported in the literature (Li et al., 2014; Li et al., 2016).

Impregnation of the IL into the ZIF-8 structure was confirmed by IL assignments found in the respective IL@ZIF-8 composite spectrum. Interestingly, the composites $[C_2MIM][Ac]$@ZIF-8, $[C_2MIM][Val]$@ZIF-8, $[C_2MIM][Cap]$@ZIF-8 and $[C_2MIM]_2[Glu]$@ZIF-8 did not present any strong IL-related bands, with their spectra almost overlapping with the ZIF-8 one. Nevertheless, two very weak bands between 655 and 615 cm^{-1} could be found in all neat ILs and respective composites spectra, but not in the MOF spectrum (see insets of Figures S13-S20). These bands have been attributed to rocking in-plane and out-of-plane deformation vibrations of the carboxylate ion (Socrates, 2004), and confirmed IL impregnation in all composite materials. Other IL-related bands with significant blue shifts (increase in the wavenumber) were found in $[C_2MIM][For]$@ZIF-8 (1632 cm^{-1}, asymmetric carboxylate ion stretching, +33 cm^{-1} blue shift), $[C_2MIM][TfAc]$@ZIF-8 (1690 cm^{-1}, carboxylate ion stretching, +7 cm^{-1} blue shift), $[C_2MIM][Lev]$@ZIF-8 (1713 cm^{-1}, γ-ketocarboxylate ion stretching, +7 cm^{-1} blue shift) and $[C_2MIM]_2[Oxa]$@ZIF-8 (doublet structure with bands at 1610 and 1673 cm^{-1}, asymmetric carboxylate ion stretching, respective +73 and +99 cm^{-1} blue shift) (Socrates, 2004). These significant blue shifts revealed the presence of IL-MOF interactions that induce the contraction of the carboxylate ion bonds, and likely indicate post-impregnation changes in the electronic density of the materials (Kinik et al., 2016).

3.2. TGA

Figure S21 (*See* SI) shows the obtained thermograms of ZIF-8, pure ILs, and respective IL@ZIF-8 composites. ZIF-8 and neat ILs showed a single mass loss stage, whereas for all composites two stages were visible. The first stage was related to the thermal decomposition of the impregnated IL, and the second stage was related to the thermal degradation of the ZIF-8 organic ligand. In this work, it was defined T_{start} as the temperature at which mass loss of a degassed sample gets to 1 wt.%. As seen in Table 1, ZIF-8 started to thermally degrade at much higher temperatures than the other materials. All IL@ZIF-8 composites impregnated with a monocarboxylate anion showed slightly higher T_{start} values when compared to the respective IL. This is true even when a fluorinated moiety or ketone group is found in the anion. The T_{start} difference was 21 ± 3 K and indicates that IL degradation in the composite was slower than that of the neat IL. This tendency was already reported in a previous paper of the group for a $[C_2MIM][Ac]$@ZIF-8 composite with a low IL loading (7.1 wt.%) (Ferreira et al., 2019). The presence of methyl and methylene groups in the IL anion was important for T_{start} increase. For example, formate-based systems (neat IL and composite) started to decompose earlier than acetate-, valerate- and caprate-based systems. Interestingly, for dicarboxylate anions, the T_{start} difference was not as meaningful as for monocarboxylate anions. Actually,

Table 1
Impregnated IL loading, starting degradation temperatures, and remaining sample amount – experimental and expected, using Eq. (6) – of ZIF-8, pure ILs, and IL@ZIF-8 composites, at 1273 K.

Sample	IL loading (wt.%)	T_{start} (K)	Experimental remaining sample amount (wt.%)	Expected remaining sample amount (wt.%)
ZIF-8	–	708	49	–
$[C_2MIM][For]$	–	443	9	–
$[C_2MIM][For]$@ZIF-8	9.3	461	49	45
$[C_2MIM][Ac]$	–	462	7	–
$[C_2MIM][Ac]$@ZIF-8	10.0	483	49	45
$[C_2MIM][TfAc]$	–	429	9	–
$[C_2MIM][TfAc]$@ZIF-8	12.8	447	48	44
$[C_2MIM][Val]$	–	457	4	–
$[C_2MIM][Val]$@ZIF-8	12.2	480	46	44
$[C_2MIM][Lev]$	–	470	10	–
$[C_2MIM][Lev]$@ZIF-8	12.9	492	47	44
$[C_2MIM][Cap]$	–	465	8	–
$[C_2MIM][Cap]$@ZIF-8	15.6	489	43	43
$[C_2MIM]_2[Oxa]$	–	471	4	–
$[C_2MIM]_2[Oxa]$@ZIF-8	16.8	474	45	41
$[C_2MIM]_2[Glu]$	–	464	28	–
$[C_2MIM]_2[Glu]$@ZIF-8	18.7	458	46	45

$[C_2MIM]_2[Glu]$@ZIF-8 showed inferior T_{start} to its respective neat IL, while for oxalate-based systems T_{start} values were similar. It is possible, akin to the scorpion-like interactions between the imidazolium ring and bulky side alkyl chains (Shimizu et al., 2013), that larger monocarboxylates have structural flexibility. In the case of the dicarboxylate ILs, the fact that the two IL cations will interact with both ends of the anionic structure does not allow for such structural flexibility. The shifts in T_{start} between neat IL and composite material indicate the existence of IL-MOF interactions, consistent with FT-IR data. Depending on the nature of the anion, these interactions seem to be different and could be indicative of distinct post-impregnation IL arrangements in the MOF structure.

The calculated TGA profiles of the composite materials were obtained from the experimental TGA thermograms of the precursor materials and IL loading, at a given temperature according to

$$\text{Calc. wt.\%}|_T = \text{wt.\%}_{\text{ZIF-8}}|_T \times \left(1 - \text{wt.\% loading}_{\text{IL}}\right) + \text{wt.\%}_{\text{IL}}|_T \times \text{wt.\% loading}_{\text{IL}}. \quad (6)$$

As seen in Figure S21 (*See* SI), the calculated composite profile can reasonably predict the experimental one, particularly after 673 K. This suggests that carboxylate-based ILs do not generate degradation products that accelerate the thermal degradation of ZIF-8 (Ferreira et al., 2019; Ferreira et al., 2023). Significant differences between the two profiles are only observed in the IL degradation step, where most composite thermograms show a slower degradation rate than the calculated ones (the blue curve is shifted to the right of the green curve). The $[C_2MIM][For]$@ZIF-8 composite is the sole exception to this trend.

The calculated and experimental remaining sample amounts were also compared. As shown in Table 1, these differences were not so significant, and the calculated values were always inferior to the experimental ones. This seems to reinforce the idea that the thermal degradation products of these carboxylate-based ILs, with these loadings, do not accelerate ZIF-8 thermal decomposition.

3.3. Textural properties of IL@ZIF-8 composites

Different textural properties of ZIF-8 and IL@ZIF-8 composites were assessed from N_2 sorption-desorption data at 77 K (*See* SI, Figures S22 and S23). The total pore volumes (V_p) of the materials were determined at a relative pressure of 0.97, and their micropore volumes ($V_{micropore}$) were calculated using the Dubinin-Astakhov equation (Do, 1998). Finally, the BET and Langmuir specific surface areas (A_{BET} and $A_{Langmuir}$, respectively) of the materials were also calculated. These properties are shown in Table 2, together with the experimentally determined solid matrix density (ρ_s) of each material. The textural properties of ZIF-8 were in agreement with the literature (Park et al., 2006; Toyao et al., 2015; Cao et al., 2013). The N_2 isotherms were all Type I according to the IUPAC classification (Thommes et al., 2015), denoting the microporous nature of the MOF precursor and the produced composites. This was corroborated by the calculated micropore volumes of these materials, which made up 96–99 % of the determined pore volume.

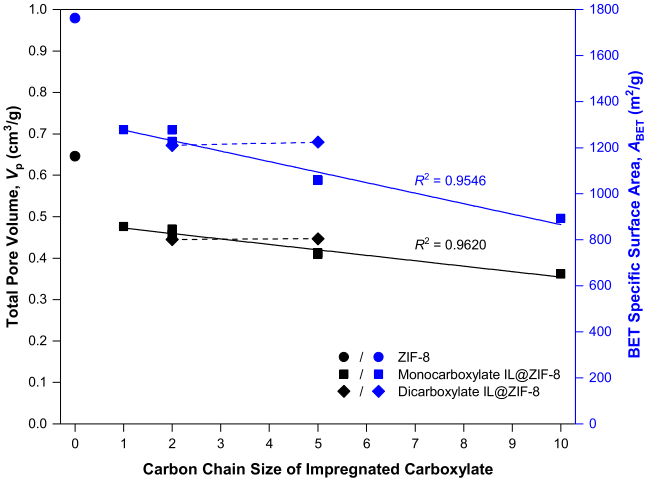

Fig. 2. Relationship between carbon chain size of impregnated carboxylate and textural properties for different IL@ZIF-8 systems. Solid and dashed lines are guide-to-the-eye that relate the total pore volume and BET specific surface area with the carbon chain size of the impregnated IL for monocarboxylate- and dicarboxylate-based IL@ZIF-8 composites, respectively.

From the data shown in Table 2, it was possible to confirm the impact of IL impregnation on the textural properties of the composites. When compared to ZIF-8, these materials lost 26–44 % of total pore volume and showed respective BET and Langmuir specific surface areas losses of 28–49 % and 27–49 %. This can be explained by IL occupation/blockage of free sorption sites in the ZIF-8 structure. Interestingly, there was a relationship between textural properties loss and the carbon chain size of the impregnated carboxylate. As an example, the $[C_2MIM][Cap]$@ZIF-8 composite, with a C10 carboxylate, experienced higher textural properties losses than $[C_2MIM][Val]$@ZIF-8 (C5 carboxylate) or $[C_2MIM][Ac]$@ZIF-8 (C2 carboxylate). As shown in Fig. 2,

Table 2
Textural properties of ZIF-8 and the IL@ZIF-8 composites, obtained by N_2 sorption-desorption equilibrium at 77 K, and their solid matrix density, determined by He pycnometry at 333 K. The values in brackets are in an IL-free basis, expressed per gram of ZIF-8.

Sample	V_p (cm^3/g)	$V_{micropore}$ (cm^3/g)	A_{BET} (m^2/g)	$A_{Langmuir}$ (m^2/g)	ρ_s (g/cm^3)
ZIF-8	0.646	0.618	1763	1812	1.41
$[C_2MIM][For]$@ZIF-8	0.476 (0.525)	0.465 (0.513)	1278 (1409)	1321 (1456)	1.35
$[C_2MIM][Ac]$@ZIF-8	0.470 (0.522)	0.461 (0.512)	1277 (1419)	1323 (1470)	1.39
$[C_2MIM][TfAc]$@ZIF-8	0.457 (0.524)	0.438 (0.502)	1227 (1407)	1267 (1453)	1.35
$[C_2MIM][Val]$@ZIF-8	0.412 (0.469)	0.402 (0.458)	1059 (1206)	1102 (1255)	1.25
$[C_2MIM][Lev]$@ZIF-8	0.409 (0.470)	0.400 (0.459)	1057 (1214)	1104 (1268)	1.36
$[C_2MIM][Cap]$@ZIF-8	0.362 (0.429)	0.349 (0.414)	893 (1058)	923 (1094)	1.28
$[C_2MIM]_2[Oxa]$@ZIF-8	0.449 (0.540)	0.445 (0.535)	1210 (1454)	1240 (1490)	1.28
$[C_2MIM]_2[Glu]$@ZIF-8	0.451 (0.555)	0.447 (0.550)	1224 (1506)	1278 (1572)	1.31

there was an almost linear dependence (*See* solid lines) between the obtained total pore volume and the BET specific surface area with the carbon chain size of the impregnated monocarboxylate. The composites $[C_2MIM]_2[Oxa]$@ZIF-8 and $[C_2MIM]_2[Glu]$@ZIF-8 did not reveal this relationship (*See* dashed lines), with textural properties being independent of the carbon chain size of the impregnated dicarboxylate.

Note that the standard BET data treatment should only consider N_2 sorption-desorption data points between the relative pressure range of 0.05–0.30. Typically, this condition cannot be met for microporous materials, which is why the low-pressure range was herein enlarged and included in calculations (Thommes et al., 2015). Because of this, Langmuir analysis is preferred for materials with microporous nature. As shown in Table 2, BET and Langmuir specific surface areas are similar, with the Langmuir model slightly overestimating this property.

To understand the impact of the impregnated IL anionic structure, the textural properties of the composites must be determined per gram of ZIF-8 in each material (i.e., in an IL-free basis). These values can be seen in Table 2, and they all were still inferior to the textural properties of pristine ZIF-8, which confirmed that all ILs occupy/block free sorption sites. If the IL was fully outside the MOF structure (e.g., it is too big to fit in the pore aperture), the total pore volume in IL-free basis of this hypothetical composite would be the same as the pristine ZIF-8. Also, in IL-free basis, it was confirmed that the textural properties of $[C_2MIM]_2[Oxa]$@ZIF-8 and $[C_2MIM]_2[Glu]$@ZIF-8 are independent of the carbon chain size of the impregnated dicarboxylate. This, along with FT-IR and TGA results, reinforces the idea that these two dicarboxylate-based ILs have different interactions with the ZIF-8 structure, and are arranged in a different manner when compared to the monocarboxylate-based ILs produced in this work. Considering their higher IL-free textural properties it is possible that, by comparison, more IL is found outside the ZIF-8 structure while not blocking/occupying so much available pore volume. From this interpretation, however, it should not be understood that these two dicarboxylate-based ILs are fully outside the ZIF-8 structure.

The PSDs of pristine ZIF-8 and IL@ZIF-8 composites were also determined, using NLDFT calculations. These distributions, shown in Figure S24 (*See* SI), showed essentially a similar distribution as ZIF-8, but with decreased available pore volume. They also confirmed the microporous nature of the produced composites (all pores have <20 Å width) (Thommes et al., 2015).

3.4. PXRD

The impregnation protocol should not affect the structural integrity of the MOF. To confirm this, diffractograms of ZIF-8 and IL@ZIF-8 composites were obtained, as shown in Figure S25 (*See* SI). The ZIF-8 diffractogram was similar to others reported in the literature (Song et al., 2015; Yurderi et al., 2014), and the IL@ZIF-8 ones overlapped it (i.e., there was no change in the peak positions). This indicates that no noticeable structural changes in the ZIF-8 structure were found in the composites after IL impregnation. Therefore, the crystallinity of ZIF-8 was preserved after this process.

PXRD data of IL@ZIF-8 composites showed that a peak found at 16.4 ° had a higher intensity than the peak found in the ZIF-8 diffractogram for the same 2θ value. This corroborates the FT-IR results that possibly pointed to changes in the electron density of the composites after IL impregnation (Kinik et al., 2016). These changes are the result of the established IL-MOF interactions revealed by FT-IR and TGA data.

3.5. Sorption performance of IL@ZIF-8 materials

The gas sorption performance of IL@MOF composites generically depends on the combination of different factors, such as the MOF/IL system and the IL loading, pore volume loss from IL occupation/blockage, possible synergistic effects, and the solvent used for impregnation. This last factor should not be overlooked and, in the ZIF-8 case, it was previously shown that ethanol does not affect the sorption capacity of this MOF, nor its structural integrity (Ferreira et al., 2020). The gas sorption-desorption data of ZIF-8 and IL@ZIF-8 composites can be found in Tables S1-S5 (*See* SI).

Single-component CO_2 and N_2 sorption-desorption equilibrium isotherms for ZIF-8 and all monocarboxylate-based IL@ZIF-8 composites were measured at 303 K and are shown in Fig. 3.

The isotherms were all Type I, according to IUPAC classification (Thommes et al., 2015), even though the low-pressure profile of some isotherms was not linear. In these cases, the first sorption point corresponded to a large gas uptake (due to the IL presence). The classical Type I shape started from the second sorption point. This kind of isotherm profile has already been reported for carboxylate-based IL@MOF materials (Mohamedali et al., 2019; Mohamedali et al., 2018) and can be explained by the high CO_2 solubility of these ILs at low pressures (0–1 bar) (Yokozeki et al., 2008). That is the case of $[C_2MIM][Ac]$, which showed the atypical Type I isotherm shape for CO_2 at this pressure range, due to chemical reaction between the IL and the gas (Yokozeki et al., 2008; Shiflett and Yokozeki, 2009; Gómez-Coma et al., 2014). While different reactional mechanism have been proposed (Maginn, 2005; Gurau et al., 2011; Mao et al., 2016), the reaction between the $[C_nMIM][Ac]$ IL and CO_2 increases the sorption capacity of this gas at low pressures in imidazolium-based ILs (Avila et al., 2021) and, by extension, in imidazolium-based IL@ZIF-8 composites. This reaction was expected to occur with other monocarboxylates. As a counterpoint, $[C_2MIM][TfAc]$ showed a largely linear CO_2 solubility profile (Yokozeki et al., 2008), consistent with the classical Type I (linear) profile of its respective composite between 0 and 1 bar. Also, despite the composite $[C_2MIM][For]$@ZIF-8 having an impregnated IL with a carboxyl group in its anion, its isotherm was a classical Type I. Both $[C_2MIM][TfAc]$ and $[C_2MIM][For]$ seem to have weak, physical interactions with CO_2. This suggests that the presence of an alkyl chain in carboxylate-based ILs is important to obtain non-linear CO_2 solubility profiles, that indicate stronger interactions (possibly physic-

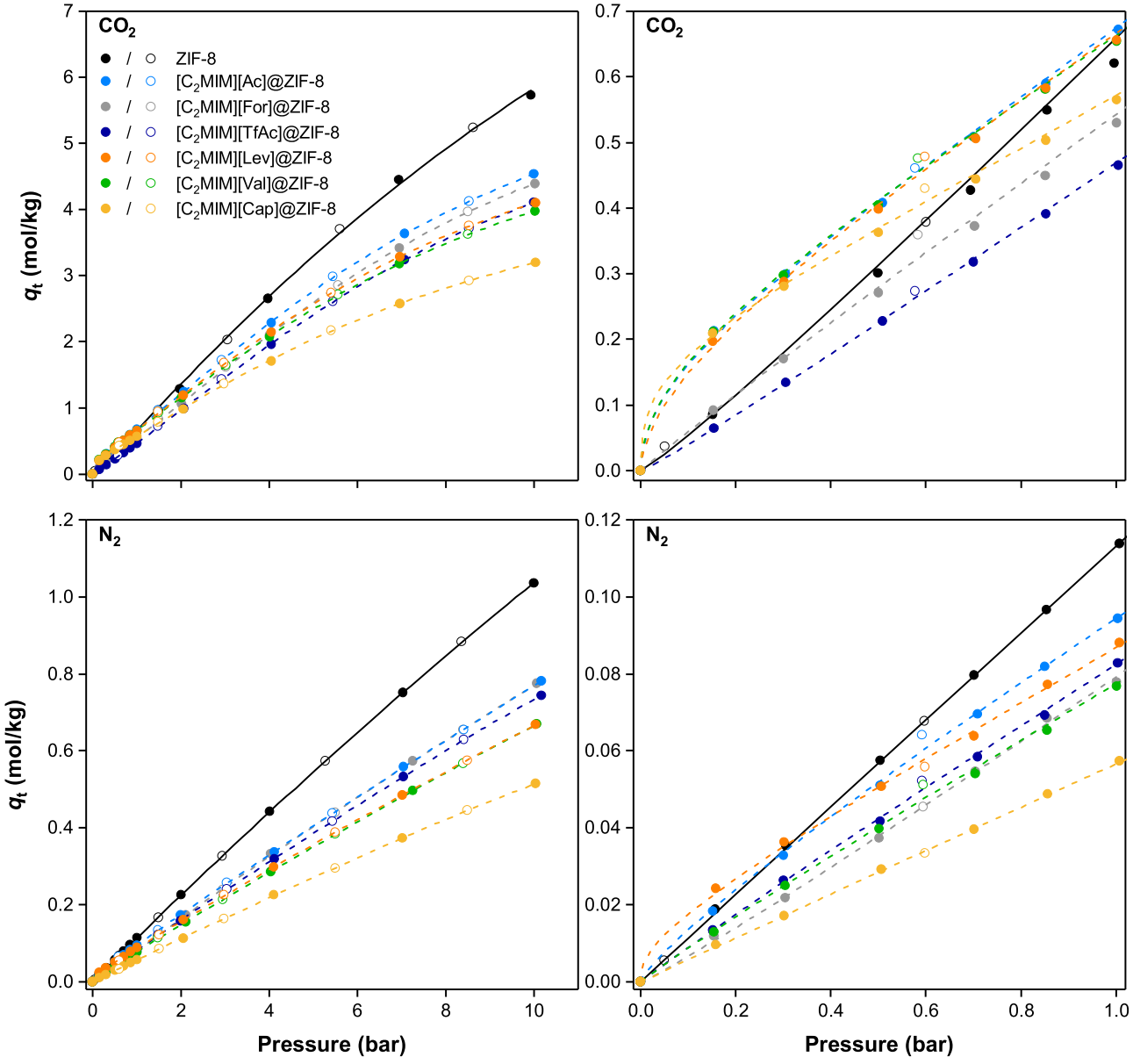

Fig. 3. (Left) Single-component sorption-desorption equilibrium isotherms of CO_2 and N_2 for ZIF-8 and monocarboxylate-based IL@ZIF-8 composites at 303 K. Closed and open symbols denote sorption and desorption data, respectively. Lines represent the Sips (ZIF-8) and dual-site Sips (composites) isotherm models fittings to the experimental data points. (Right) Low-pressure range insets of the data are shown to clarify the goodness of the fittings to the experimental data.

ochemical ones) with the gas. Consequently, IL@ZIF-8 composites impregnated with these ILs will likely show higher CO_2 sorption capacity between 0 and 1 bar. All composites, except [C_2MIM][For]@ZIF-8 and [C_2MIM][TfAc]@ZIF-8, showed superior CO_2 sorption capacity than pristine ZIF-8 up until 0.7 bar. For N_2, only [C_2MIM][Lev]@ZIF-8 and [C_2MIM][Ac]@ZIF-8 showed superior sorption capacity than the MOF, and only up until 0.3 bar. So, despite pore volume loss, the impregnated ILs have introduced new, stronger sorption sites in the composite materials.

Surprisingly, at 0.15 bar, the CO_2 gas sorption capacity in [C_2MIM][Ac]@ZIF-8, [C_2MIM][Val]@ZIF-8 and [C_2MIM][Cap]@ZIF-8 composites proved to be independent of the IL anionic carbon chain size. This trend was not observed for this pressure in N_2 sorption, where shorter chains benefitted the gas sorption capacity. For higher pressures, shorter anionic carbon chains also benefited CO_2 sorption. This trend was already observed in a previous work by the group for imidazolium side alkyl chains in bistriflimide-based ILs (Ferreira et al., 2019). Finally, by comparing the sorption performance of [C_2MIM][Val]@ZIF-8 with [C_2MIM][Lev]@ZIF-8, the additional ketone group in the latter composite only had a significant impact in N_2 sorption between 0 and 1 bar, with CO_2 sorption capacity being similar in the entire pressure range.

Single-component CO_2 and N_2 sorption-desorption equilibrium isotherms for dicarboxylate-based IL@ZIF-8 composites were also measured at 303 K (Fig. 4) and compared with monocarboxylate-based composites with the same carbon chain size.

The isotherms of dicarboxylate-based composites were Type I, according to IUPAC classification (Thommes et al., 2015), but with the same atypical, non-linear profile at low pressures as monocarboxylate-based composites. The classical Type I shape started around 0.5 bar.

The dicarboxylate-based IL@ZIF-8 materials revealed high N_2 sorption at low-pressure, with the uptake of this gas being at least doubled at 0.15 bar, when compared to monocarboxylate-based IL@ZIF-8 composites. At the same pressure, [C_2MIM]$_2$[Glu]@ZIF-8 also showed around

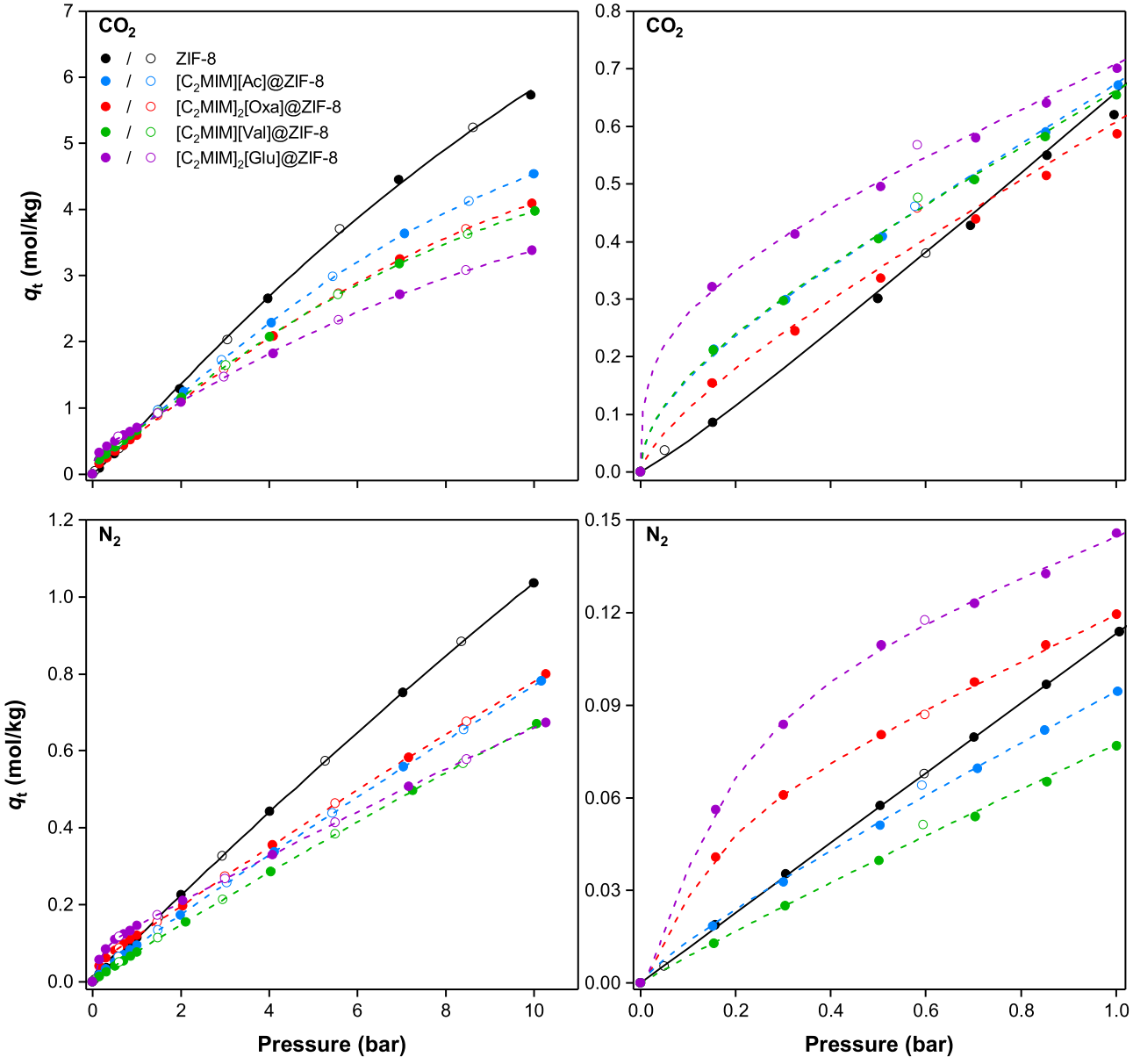

Fig. 4. (Left) Single-component sorption-desorption equilibrium isotherms of CO_2 and N_2 for ZIF-8 and mono- and dicarboxylate-based IL@ZIF-8 composites at 303 K. Closed and open symbols denote sorption and desorption data, respectively. Lines represent the Sips (ZIF-8) and dual-site Sips (composites) isotherm models fittings to the experimental data points. (Right) A low-pressure range inset of the data is shown to clarify the goodness of the fittings to the experimental data.

50 % more CO_2 sorption than [C_2MIM][Ac]@ZIF-8. This is consistent with solubility data of this gas reported in the literature for similar ILs ([C_4MIM]$_2$[Glu] and [C_4MIM][Ac]), where the dicationic IL showed at least double of CO_2 molar fraction between 0 and 1 bar (Avila et al., 2021). Interestingly, at this same pressure range, [C_2MIM]$_2$[Oxa]@ZIF-8 showed less CO_2 sorption capacity than the monocarboxylate-based composites. This reinforces the idea, analogous to [C_2MIM][For] IL, that an alkyl chain in the middle of the two carboxyl groups is important in dicarboxylate-based ILs to increase CO_2 solubility.

The isotherms in Fig. 4 revealed the experimentally obtained sorption-desorption collected data. An IL-free basis (i.e., gas sorption capacity normalized per unit mass of ZIF-8) was once again used to obtain more information about the IL impact on the sorption capacity of the composites. Note that the same IL moles were impregnated for all IL@ZIF-8 materials. For a given gas, if ILs did not affect the gas sorption capacity, all isotherms should collapse into a single one in IL-free basis. Furthermore, the same pore volume loss would be observed in all composites, as constant molar loading was impregnated. This was not verified by N_2 data at 77 K, which means that IL gas solubility and structures, and the distinct incorporation mechanism into the ZIF-8 matrix do have an impact on the gas sorption capacity for these composites. Figures S26 and S27 (*See* SI) present the CO_2 and N_2 IL-free isotherms, and from them, it can be seen that ILs had a negative impact on the gas sorption capacity, for pressures above 1 bar. Considering that no IL-free isotherms overlapped the ZIF-8 ones, it further confirms ILs are occupying/blocking available MOF pore volume. Bulkier carboxylates, as found in [C_2MIM][Cap]@ZIF-8, were the ones that affected gas sorption capacity the most. These anionic alkyl chains may have higher flexibility and block gas access to the available pore volume, as suggested in our previous study for composites impregnated bistriflimide-based ILs with bulky imidazolium cations (Ferreira et al., 2019).

Another way to look at the sorption-desorption data collected herein is to determine the sorption capacity of the materials per available pore

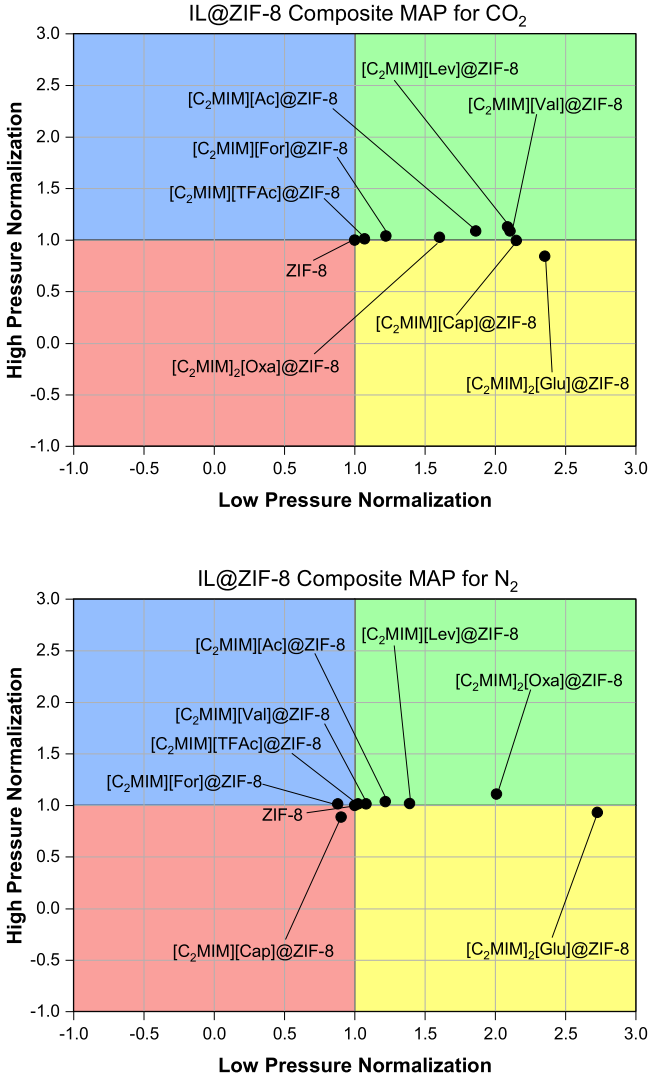

Fig. 5. MAP of IL@ZIF-8 composites for the sorption of CO_2 and N_2 at 303 K. ZIF-8 is the normalization reference assumed in the MAP calculation for both low- and high-pressure normalizations (reference pressures of 0.5 and 10 bar, respectively).

volume. This can be achieved by dividing the sorption gas amount of the material by its measured total pore volume. A sorbed amount (q_t/V_p), expressed in mol gas/cm^3 of available pore volume, is obtained and the calculated isotherms are shown in Figure S28 (*See* SI). It can be observed that the IL impregnation led to a higher sorption capacity of CO_2 per available cm^3 of pore volume in monocarboxylate-based composites, whereas N_2 sorption was very similar to the pristine ZIF-8 (or worse, in the case of [C_2MIM][Cap]@ZIF-8). As for the dicarboxylate-based composites, [C_2MIM]$_2$[Oxa]@ZIF-8 showed slightly higher sorption capacity than ZIF-8, while [C_2MIM]$_2$[Glu]@ZIF-8 started by sorbing more than the MOF in the low pressures but eventually was outperformed at high pressures. The q_t/V_p composites data were normalized using the pristine ZIF-8 as reference material. This was done by dividing the $q_t/V_p = f(P)$ of every composite by the respective q_t/V_p of ZIF-8. The normalized values for 0.5 and 10 bar (representative of low- and high-pressure regimes, respectively) for the two gases are presented in Tables S6 and S7 (*See* SI). The same data can be observed in Fig. 5 for ZIF-8 and composites. The analysis of the quadrants for both CO_2 and N_2 indicated once again that all the produced composites herein, for the most part, displayed interesting differences in normalized sorption data in the low-pressure regime (green and yellow MAP quadrants). However, at high pressure, the normalized value was close to one in all cases, denoting a negligible effect of the IL in the composite. More specifically, there was an effect of the anionic carbon chain size for CO_2; the bigger the chain, the higher the normalized values. The [C_2MIM]$_2$[Glu]@ZIF-8 composite had the highest normalized values in the low-pressure regime for both gases, being the composite that sorbed the most of the two sorbates. The composite [C_2MIM][Cap]@ZIF-8 showed inferior N_2 normalized sorption data to ZIF-8 for both pressure regimes (red MAP quadrant). This change in quadrants is indicative of higher selectivity of this material at low pressures. Imidazolium-based ILs can be used to tailor selectivity to IL@ZIF-8 composites, and these materials are more selective at low pressures if their cation or anion has large alkyl chains (Ferreira et al., 2019).

To determine the selectivity performance of the materials, ZIF-8 and IL@ZIF-8 sorption-desorption data were fitted with Sips and dual-site Sips fittings, respectively. Given that the ILs impregnation led to atypical Type I isotherms, the dual-site Sips model was preferred for the composite materials. This model considers sorption sites with different energies, which seems appropriate for these IL@ZIF-8 composites, given the existence of both carboxylate ILs and MOF sorption sites (Yang et al., 2021). The obtained model fitting parameters can be found in Tables S8 and S9 (*See* SI). ZIF-8 showed an expected higher maximum sorbed amounts and affinity for CO_2 than for N_2, while presenting a homogeneous system as n was close to 1. The general trend in composites was that the sorption site 1, attributed to ZIF-8 sorption sites, had higher maximum sorbed amounts than those of sorption site 2, attributed to the IL sorption. In fact, N_2 sorption-desorption in [C_2MIM][Ac]@ZIF-8 was the only case in which $q_{s1} < q_{s2}$. In many cases, q_{s1} was far superior to q_{s2}, meaning ZIF-8 sorption sites were the ones contributing the most to high-pressure gas sorption. Also, b_1 and b_2 parameters for CO_2 were always superior to the same parameters for N_2. The sole exceptions were for the b_2 parameters of [C_2MIM][Cap]@ZIF-8, [C_2MIM]$_2$[Oxa]@ZIF-8 and [C_2MIM]$_2$[Oxa]@ZIF-8. This was deemed as a mathematical artifice caused while trying to find the best fitting for the isotherms. Given that these three composites sorbed more CO_2 than N_2, it is unrealistic that their affinity towards the former gas is inferior when compared to the latter gas. Finally, in composites in which atypical Type I CO_2 isotherms were found, it was observed that $n_1 < n_2$. This means the ILs are contributing to making the system more heterogeneous, as expected. This trend is not observed for [C_2MIM][For]@ZIF-8 and [C_2MIM][TfAc]@ZIF-8, the two composites with more linear isotherms between 0 and 1 bar. For N_2 this trend was noticeable and $n_1 > n_2$, except for [C_2MIM][Lev]@ZIF-8. This exception was considered again as a mathematical artifice created by the shape of the isotherm.

From the obtained fittings, it was possible to calculate ideal the CO_2/N_2 selectivity, considering post-combustion flue gas composition (15 vol.% CO_2:85 vol.% N_2), as shown in Fig. 6. All the produced composites, except [C_2MIM][TfAc]@ZIF-8, showed superior CO_2/N_2 selectivity than ZIF-8 for the entire total pressure range. The composite [C_2MIM][Cap]@ZIF-8 showed the highest selectivity value at 1 bar of all the composites and was nearly five times more selective than ZIF-8 at this pressure. In fact, the larger the anionic carbon chain size, the higher the selectivity at 1 bar. Note that this is the pressure condition of post-combustion CO_2 capture/separation. The composite [C_2MIM][Lev]@ZIF-8 showed slightly inferior selectivity up to 4 bar than [C_2MIM][Val]@ZIF-8 ([C_2MIM][Lev] has an additional ketone group when compared to [C_2MIM][Val]). This can be explained by the N_2 sorption capacity of [C_2MIM][Lev]@ZIF-8 at low pressures. The two composites that sorbed less CO_2, namely [C_2MIM][For]@ZIF-8 and [C_2MIM][TfAc]@ZIF-8, were the ones closest to the ZIF-8 selectivity profile. In the latter composite, the addition of the IL did not improve the selectivity performance of the material, when compared to the pristine ZIF-8. Regarding the dicarboxylate-based composites, their high N_2 sorption capacity made these materials less selective than the monocarboxylate-based composites with the same carbon chain size.

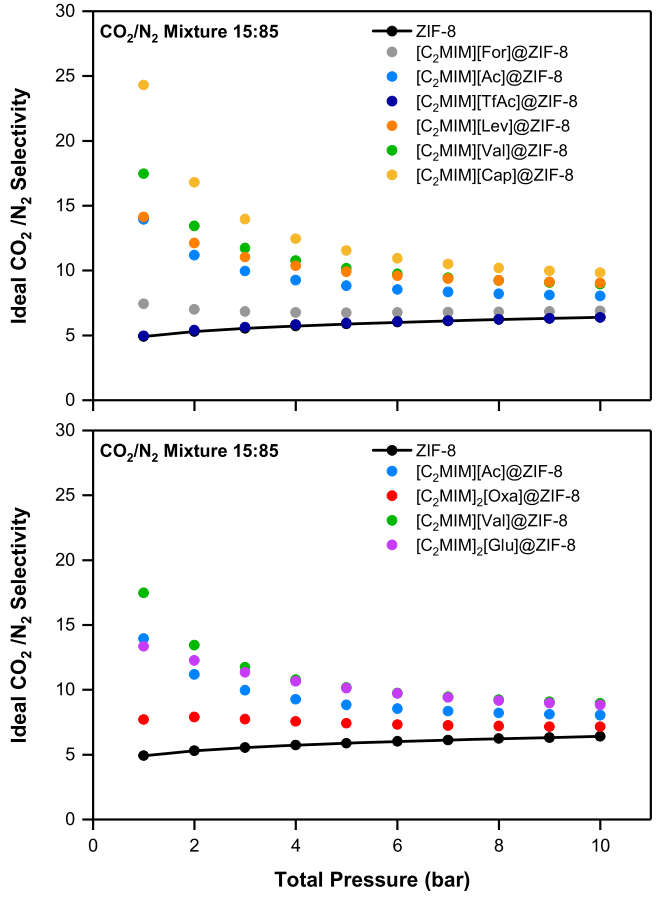

Fig. 6. Ideal CO_2/N_2 selectivity for the pristine ZIF-8 and IL@ZIF-8 composites as a function of the total mixture pressure, determined from the Sips (ZIF-8) and dual-site Sips (composites) adsorption isotherm models of the single-component sorption-desorption isotherms, measured at 303 K and in the pressure range of 0.5–10 bar. The line is a guide-to-the-eye relative to the pristine ZIF-8.

4. Conclusions

In this work, the anionic effect on gas sorption and selectivity performance of the produced IL@ZIF-8 composites was studied. A total of eight mono- and dicarboxylate-based ILs were used to impregnate the MOF ZIF-8 targeting CO_2 post-combustion separation.

FT-IR data confirmed the IL impregnation into the structure of ZIF-8, and significant blue shifts were the result of IL-MOF interactions, also confirmed by TGA data. From N_2 sorption-desorption data at 77 K, it was found that IL@ZIF-8 composites presented lower textural properties than ZIF-8. An almost linear relationship between the anionic carbon chain size and the textural properties was found for monocarboxylate-based IL@ZIF-8 composites. For the dicarboxylate-based ones included in this work, their textural properties were independent of the anionic carbon chain size. PXRD diffractograms of all the materials showed structure and crystallinity conservations after the IL impregnation protocol.

The single-component sorption-desorption isotherms of CO_2 obtained at 303 K were atypical Type I ones for most composites. At 0.15 bar, almost all composites showed superior CO_2 sorption from ZIF-8, which means that most of the impregnated ILs introduced new and stronger sites for gas sorption (chemisorption ILs that promoted reaction with CO_2). The dicarboxylate-based composites showed remarkable increases in N_2 sorption. Moreover, $[C_2MIM]_2[Glu]$@ZIF-8 showed a 50 % increase in CO_2 sorption at 0.15 bar compared to both $[C_2MIM][Ac]$@ZIF-8 and $[C_2MIM][Val]$@ZIF-8, the latter being its corresponding monocarboxylate composite.

Except for $[C_2MIM][TfAc]$@ZIF-8, all composites showed superior ideal CO_2/N_2 selectivity for the entire total pressure range (0–10 bar), when compared to ZIF-8. It was observed at 1 bar that the larger the IL anionic carbon chain size, the more selective the material is. Specifically, $[C_2MIM][Cap]$@ZIF-8 showed a nearly five times selectivity increase, when compared to ZIF-8. The dicarboxylate-based composites, given their high N_2 sorption at low pressure, were less selective than the monocarboxylate-based composites with the same carbon chain size.

This work expands the list of IL@MOF composites produced for gas sorption applications and reaffirms that carboxylate-based IL@MOF are interesting candidates to be used for CO_2 post-combustion capture/separation.

Declaration of competing interest

The authors declare that they have no known competing financial interests or personal relationships that could have appeared to influence the work reported in this paper.

CRediT authorship contribution statement

Tiago J. Ferreira: Writing – review & editing, Writing – original draft, Methodology, Investigation. **Thiago O. Carvalho:** Writing – review & editing, Methodology, Investigation. **Joana Pais:** Writing – review & editing, Investigation. **Laura M. Esteves:** Writing – review & editing, Writing – original draft, Methodology, Investigation. **Ludmila P.C. Silva:** Investigation. **Patrícia M. Reis:** Writing – review & editing, Methodology. **José M.S.S. Esperança:** Writing – review & editing, Supervision, Resources, Project administration, Methodology, Investigation, Funding acquisition, Conceptualization. **Isabel A.A.C. Esteves:** Writing – review & editing, Supervision, Resources, Project administration, Methodology, Investigation, Funding acquisition, Conceptualization.

Acknowledgments

The authors thank Fundação para a Ciência e Tecnologia, FCT/MCTES (Portugal), for financial support through PhD grants SFRH/BD/139627/2018 and COVID/BD/152969/2023 (T. J. F.), PhD grant 2021.07148.BD (T. O. C.), FCT Investigator contract (2021.00511.CEECIND – P. M. R), project PTDC/CTM-CTM/30326/2017 and Material Characterization Laboratory (LAMATE/UFF) for obtaining the PXRD diffractograms. Additionally, the work was also partially supported by the Associate Laboratory for Green Chemistry, LAQV, which is funded by national funds from FCT/MCTES (10.54499/UIDB/50006/2020, 10.54499/UIDP/50006/2020 and 10.54499/LA/P/0008/2020). The NMR spectrometers are part of The National NMR Facility, supported by FCT/MCTES (Grant RECI/BBB-BQB/0230/2012).

Supplementary materials

Supplementary material associated with this article can be found, in the online version, at doi:10.1016/j.ccst.2024.100282.

References

Avila, J., Lepre, L.F., Santini, C.C., Tiano, M., Denis-Quan-quin, S., Szeto, K.C., et al., 2021a. High-performance porous ionic liquids for low-pressure CO_2 capture. Angew. Chem. Int. Ed. 60, 12876–12882. doi:10.26434/chemrxiv.13382741.v1.

Avila, J., Lepre, L.F., Goloviznina, K., Guazzelli, L., Pomelli, C.S., Chiappe, C., et al., 2021b. Improved carbon dioxide absorption in double-charged ionic liquids. Phys. Chem. Chem. Phys. 23, 23130–23140. doi:10.1039/d1cp02080c.

Ban, Y., Li, Z., Li, Y., Peng, Y., Jin, H., Jiao, W., et al., 2015. Confinement of ionic liquids in nanocages: tailoring the molecular sieving properties of ZIF-8 for membrane-based CO_2 capture. Angewandte Chemie - Int. Ed. 54, 15483–15487. doi:10.1002/anie.201505508.

Batten, S.R., Champness, N.R., Chen, X.-M., Garcia-Martinez, J., Kitagawa, S., Öhrström, L., et al., 2013. Terminology of metal-organic frameworks and coordination polymers. Pure Appl. Chem. 85, 1715–1724. doi:10.1351/PAC-REC-12-11-20.

Baumann, A.E., Burns, D.A., Liu, B., Thoi, V.S., 2019. Metal-organic framework functionalization and design strategies for advanced electrochemical energy storage devices. Commun. Chem. 2, 86. doi:10.1038/s42004-019-0184-6.

Boot-Handford, M.E., Abadanes, J.C., Anthony, E.J., Blunt, M.J., Brandani, S., mac Dowell, N., et al., 2014. Carbon capture and storage update. Energy Environ. Sci. 7, 130–189. doi:10.1039/c3ee42350f.

Cao, S., Gody, G., Zhao, W., Perrier, S., Peng, X., Ducati, C., et al., 2013. Hierarchical bicontinuous porosity in metal-organic frameworks templated from functional block co-oligomer micelles. Chem. Sci. 4, 3573–3577. doi:10.1039/c3sc51336j.

Carvalho, P.J., Kurnia, K.A., Coutinho, J.A.P., 2016. Dispelling some myths about the CO_2 solubility in ionic liquids. Phys. Chem. Chem. Phys. 18, 14757–14771. doi:10.1039/c6cp01896c.

Chen, Y., Hu, Z., Gupta, K.M., Jiang, J., 2011. Ionic liquid/metal-organic framework composite for CO_2 capture: a computational investigation. J. Phys. Chem. C 115, 21736–21742. doi:10.1021/jp208361p.

Chen, C., Feng, N., Guo, Q., Li, Z., Li, X., Ding, J., et al., 2018. Surface engineering of a chromium metal-organic framework with bifunctional ionic liquids for selective CO_2 adsorption: synergistic effect between multiple active sites. J. Colloid. Interface Sci. 521, 91–101. doi:10.1016/j.jcis.2018.03.029.

da Silva, F.W.M., Magalhães, G.M., Jardim, E.O., Silvestre-Albero, J., Sepúlveda-Escribano, A., de Azevedo, D.C.S., et al., 2015. CO_2 adsorption on ionic liquid-modified Cu-BTC: experimental and simulation study. Adsorp. Sci. Technol. 33, 223–242. doi:10.1260/0263-6174.33.2.223.

Do, D.D., 1998. Adsorption Analysis: Equilibria and Kinetics. Imperial College Press.

Esteves, I.A.A.C., Lopes, M.S.S., Nunes, P.M.C., Mota, J.P.B., 2008. Adsorption of natural gas and biogas components on activated carbon. Sep. Purif. Technol. 62, 281–296. doi:10.1016/j.seppur.2008.01.027.

Ferreira, T.J., Ribeiro, R.P.P.L., Mota, J.P.B., Rebelo, L.P.N., Esperança, J.M.S.S., Esteves, I.A.A.C., 2019. Ionic Liquid-Impregnated Metal-Organic Frameworks for CO_2/CH_4 Separation. ACS. Appl. Nano Mater. 2, 7933–7950. doi:10.1021/acsanm.9b01936.

Ferreira, T.J., Vera, A.T., de Moura, B.A., Esteves, L.M., Tariq, M., Esperança, J.M.S.S., et al., 2020. Paramagnetic ionic liquid/metal organic framework composites for CO_2/CH_4 and CO_2/N_2 separations. Front. Chem. 8, 590191. doi:10.3389/fchem.2020.590191.

Ferreira, T.J., Esteves, L.M., Esperança, J.M.S.S., Esteves, I.A.A.C., 2022. Unveiling the temperature influence on the sorptive behaviour of ZIF-8 composite materials impregnated with [CnMIM] $[B(CN)_4]$ ionic liquids. Processes 10, 247. doi:10.3390/pr10020247.

Ferreira, T.J., de Moura, B.A., Esteves, L.M., Reis, P.M., Esperança, J.M.S.S., Esteves, I.A.A.C., 2023. Biocompatible ammonium-based ionic liquids/ZIF-8 composites for CO_2/CH_4 and CO_2/N_2 separations. Sustain. Mater. Technol. 35, e00558. doi:10.1016/j.susmat.2022.e00558.

Gómez-Coma, L., Garea, A., Irabien, A., 2014. Non-dispersive absorption of CO_2 in [emim][EtSO4] and [emim] [Ac] : temperature influence. Sep. Purif. Technol. 132, 120–125. doi:10.1016/j.seppur.2014.05.012.

Gumma, S., Talu, O., 2010. Net adsorption: a thermodynamic framework for supercritical gas adsorption and storage in porous solids. Langmuir. 26, 17013–17023. doi:10.1021/la102186q.

Gurau, G., Rodríguez, H., Kelley, S.P., Janiczek, P., Kalb, R.S., Rogers, R.D., 2011. Demonstration of chemisorption of carbon dioxide in 1,3-dialkylimidazolium acetate ionic liquids. Angew. Chem. - Int. Ed. 50, 12024–12026. doi:10.1002/anie.201105198.

Han, G., Yu, N., Liu, D., Yu, G., Chen, X., Zhong, C., 2021. Stepped enhancement of CO_2 adsorption and separation in IL-ZIF-IL composites with shell-interlayer-core structure. AIChE J. 67, e17112. doi:10.1002/aic.17112.

Huang, M.-T., Zhai, P.-M., 2021. Achieving Paris Agreement temperature goals requires carbon neutrality by middle century with far-reaching transitions in the whole society. Adv. Clim. Change Res. 12, 281–286. doi:10.1016/j.accre.2021.03.004.

Kavak, S., Polat, H.M., Kulak, H., Keskin, S., Uzun, A., 2019. MIL-53(Al) as a versatile platform for ionic-liquid/MOF composites to enhance CO_2 selectivity over CH_4 and N_2. Chem. Asian J. 14, 3655–3667. doi:10.1002/asia.201900634.

Kinik, F.P., Altintas, C., Balci, V., Koyuturk, B., Uzun, A., Keskin, S., 2016. [BMIM] $[PF_6]$ incorporation doubles CO_2 selectivity of ZIF-8: elucidation of interactions and their consequences on performances. ACS. Appl. Mater. Interfaces. 8, 30992–31005. doi:10.1021/acsami.6b11087.

Li, H., Bhadury, P.S., Song, B., Yang, S., 2012. Immobilized functional ionic liquids: efficient, green, and reusable catalysts. RSC. Adv. 2, 12525–12551. doi:10.1039/c2ra21310a.

Li, J., Wu, Y.N., Li, Z., Zhang, B., Zhu, M., Hu, X., et al., 2014. Zeolitic imidazolate framework-8 with high efficiency in trace arsenate adsorption and removal from water. J. Phys. Chem. C 118, 27382–27387. doi:10.1021/jp508381m.

Li, D., Wu, S., Wang, F., Jia, S., Liu, Y., Han, X., et al., 2016. A facile one-pot synthesis of hemin/ZIF-8 composite as mimetic peroxidase. Mater. Lett. 178, 48–51. doi:10.1016/j.matlet.2016.04.200.

Liang, L., Liu, C., Jiang, F., Chen, Q., Zhang, L., Xue, H., et al., 2017. Carbon dioxide capture and conversion by an acid-base resistant metal-organic framework. Nat. Commun. 8, 1233. doi:10.1038/s41467-017-01166-3.

Maginn E.J. Design and evaluation of ionic liquids as novel CO2 absorbents. Quaterly Technical Report to US DOE 2005.

Mao, J.X., Steckel, J.A., Yan, F., Dhumal, N., Kim, H., Damodaran, K., 2016. Understanding the mechanism of CO2 capture by 1,3 di-substituted imidazolium acetate based ionic liquids. Phys. Chem. Chem. Phys. 18, 1911–1917. doi:10.1039/c5cp05713b.

Mohamedali, M., Ibrahim, H., Henni, A., 2018. Incorporation of acetate-based ionic liquids into a zeolitic imidazolate framework (ZIF-8) as efficient sorbents for carbon dioxide capture. Chem. Eng. J. 334, 817–828. doi:10.1016/j.cej.2017.10.104.

Mohamedali, M., Henni, A., Ibrahim, H., 2019a. Markedly improved CO_2 uptake using imidazolium-based ionic liquids confined into HKUST-1 frameworks. Microporous Mesoporous Mater. 284, 98–110. doi:10.1016/j.micromeso.2019.04.004.

Mohamedali, M., Henni, A., Ibrahim, H., 2019b. Investigation of CO_2 capture using acetate-based ionic liquids incorporated into exceptionally porous metal–organic frameworks. Adsorption 25, 675–692. doi:10.1007/s10450-019-00073-x.

Pan, R., Guo, Y., Tang, Y., Wei, D., Mengli, L., He, D., 2022. Dicationic liquid containing alkenyl modified CuBTC improves the performance of the composites: increasing the CO2 adsorption effect. Chem. Eng. J. 430, 132127. doi:10.1016/j.cej.2021.132127.

Park, K.S., Ni, Z., Côté, A.P., Choi, J.Y., Huang, R., Uribe-Romo, F.J., et al., 2006. Exceptional chemical and thermal stability of zeolitic imidazolate frameworks. Proc. Natl. Acad. Sci. u S. a 103, 10186–10191. doi:10.1073/pnas.0602439103.

Philip, F.A., Henni, A., 2022. Enhancement of post-combustion CO_2 capture capacity by incorporation of task-specific ionic liquid into ZIF-8. Microporous Mesoporous Mater. 330, 111580. doi:10.1016/j.micromeso.2021.111580.

Shi, W., Thompson, R.L., Albenze, E., Steckel, J.A., Nulwala, H.B., Luebke, D.R., 2014. Contribution of the acetate anion to CO2 solubility in ionic liquids: theoretical method development and experimental study. J. Phys. Chem. B 118, 7383–7394. doi:10.1021/jp502425a.

Shiflett, M.B., Yokozeki, A., 2009. Phase behavior of carbon dioxide in ionic liquids: [emim][acetate, emim][trifluoroacetate], and [emim][acetate] + [emim][trifluoroacetate] mixtures. J. Chem. Eng. Data 54, 108–114. doi:10.1021/je800701j.

Shimizu, K., Bernardes, C.E.S., Triolo, A., Canongia Lopes, J.N., 2013. Nano-segregation in ionic liquids: scorpions and vanishing chains. Phys. Chem. Chem. Phys. 15, 16256–16262. doi:10.1039/c3cp52357h.

Socrates, G., 2004. The Carbonyl Group: C=O. Infrared and Raman Characteristic Group Frequencies. John Wiley & Sons, Chichester, pp. 115–156.

Song, Y., Hu, D., Liu, F., Chen, S., Wang, L., 2015. Fabrication of fluorescent SiO_2@zeolitic imidazolate framework-8 nanosensor for Cu^2+ detection. Analyst 140, 623–629. doi:10.1039/c4an01773k.

Sumida, K., Rogow, D.L., Mason, J.A., McDonald, T.M., Bloch, E.D., Herm, Z.R., et al., 2012. Carbon dioxide capture in metal—organic frameworks. Chem. Rev. 112, 724–781. doi:10.1021/cr2003272.

Thommes, M., Kaneko, K., Neimark, A.V., Olivier, J.P., Rodriguez-Reinoso, F., Rouquerol, J., et al., 2015. Physisorption of gases, with special reference to the evaluation of surface area and pore size distribution (IUPAC Technical Report). Pure Appl. Chem. 87, 1051–1069. doi:10.1515/pac-2014-1117.

Toyao, T., Fujiwaki, M., Miyahara, K., Kim, T.H., Horiuchi, Y., Matsuoka, M., 2015. Design of zeolitic imidazolate framework derived nitrogen-doped nanoporous carbons containing metal species for carbon dioxide fixation reactions. ChemSusChem.ChemSusChem. 8, 3905–3912. doi:10.1002/cssc.201500780.

Venna, S.R., Carreon, M.A., 2010. Highly permeable zeolite imidazolate framework-8 membranes for CO_2/CH_4 separation. J. Am. Chem. Soc. 132, 76–78. doi:10.1021/ja909263x.

Vicent-Luna, J.M., Gutiérrez-Sevillano, J.J., Anta, J.A., Calero, S, 2013. Effect of room-temperature ionic liquids on CO_2 separation by a Cu-BTC metal-organic framework. J. Phys. Chem. C 117, 20762–20768. doi:10.1021/jp407176j.

Xia, X., Hu, G., Li, W., Li, S., 2019. Understanding reduced CO_2 uptake of ionic liquid/metal-organic framework (IL/MOF) composites. ACS. Appl. Nano Mater. 2, 6022–6029. doi:10.1021/acsanm.9b01538.

Yang, Z., Gluesenkamp, K.R., Frazzica, A., 2021. Equilibrium vapor pressure properties for absorbent and adsorbent materials. Int. J. Refrig. 124, 134–166. doi:10.1016/j.ijrefrig.2020.12.013.

Yokozeki, A., Shiflett, M.B., Junk, C.P., Grieco, L.M., Foo, T., 2008. Physical and chemical absorptions of carbon dioxide in room-temperature ionic liquids. J. Phys. Chem. B 112, 16654–16663. doi:10.1021/jp805784u.

Yurderi, M., Bulut, A., Zahmakiran, M., Gülcan, M., Özkar, S., 2014. Ruthenium(0) nanoparticles stabilized by metal-organic framework (ZIF-8): highly efficient catalyst for the dehydrogenation of dimethylamine-borane and transfer hydrogenation of unsaturated hydrocarbons using dimethylamine-borane as hydrogen source. Appl. Catal. B 160–161, 534–541. doi:10.1016/j.apcatb.2014.06.009.

Zeeshan, M., Keskin, S., Uzun, A., 2018a. Enhancing CO_2/CH_4 and CO_2/N_2 separation performances of ZIF-8 by post-synthesis modification with [BMIM] [SCN]. Polyhedron. 155, 485–492. doi:10.1016/j.poly.2018.08.073.

Zeeshan, M., Nozari, V., Yagci, M.B., Isık, T., Unal, U., Ortalan, V., et al., 2018b. Core−shell type ionic liquid/metal organic framework composite: an exceptionally high CO_2/CH_4 selectivity. J. Am. Chem. Soc. 140, 10113–10116. doi:10.1021/jacs.8b05802.

Zeeshan, M., Kulak, H., Kavak, S., Polat, H.M., Durak, O., Keskin, S., et al., 2020. Influence of anion size and electronic structure on the gas separation performance of ionic liquid/ZIF-8 composites. Microporous Mesoporous Mater. 306, 110446. doi:10.1016/j.micromeso.2020.110446.